analytical chemistry

pubs.acs.org/ac Article

Electrochemistry-Assisted Surface Plasmon Resonance Biosensor for Detection of CA 15−3

José A. Ribeiro,* Maria Goreti F. Sales, and Carlos M. Pereira*

Cite This: *Anal. Chem.* 2021, 93, 7815−7824 Read Online

ACCESS | Metrics & More | Article Recommendations | Supporting Information

ABSTRACT: In this work, we describe an innovative methodology based on combined surface plasmon resonance (SPR) and electrochemical responses (eSPR) in the same immunoassay for screening CA 15−3 cancer biomarker with high sensitivity (and selectivity), in a very simple, label-free, accurate, and fully automated manner. Detection was achieved by performing two simple steps. In the first step, direct SPR was used to monitor CA 15−3 interaction with surface immobilized antibody. Two linear response ranges were obtained and the detection limit achieved is poor (LOD of 21 U mL^{-1}). However, in the second detection step, electrochemical measurements at the SPR gold surface were performed to measure the decrease of redox probe peak current upon antigen−antibody interaction, providing a suitable amplification strategy to lower detection levels of CA 15−3 (LOD of 0.0998 U mL^{-1}), without the need of additional complex and/or expensive amplification steps to enhance the sensitivity. Moreover, selectivity studies were performed against other common cancer biomarkers and the results showed that the eSPR immunosensor is selective for the CA 15−3 protein. Finally, the clinical applicability of the developed eSPR biosensing methodology was successfully applied to detect CA 15−3 in human serum samples at clinically relevant levels due to the high sensitivity of electrochemical readout. The same concept may be further extended to other proteins of interest.

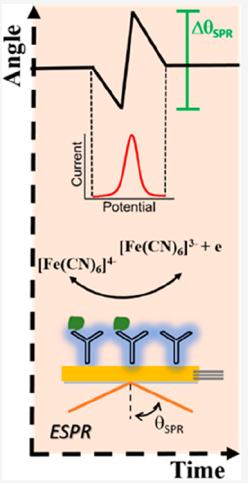

Breast cancer is by far the most common malignancy in women worldwide and the leading cause of cancer death among females, exerting tremendous physical, emotional, and financial strain on individuals, families, communities, and health systems.[1] Despite the enormous efforts to identify new circulating biomarkers for the early diagnosis, such as HER2,[2] microRNAs,[3,4] cell-free DNA,[5] only few serological tumor markers are currently used in clinical context.[6] Furthermore, Carbohydrate Antigen 15−3 (CA 15−3) is definitely the most used breast cancer biomarker, mostly in surveillance of patients with diagnosed disease and for monitoring the treatment of patients with advanced disease.[6−9] The reference range of serum CA 15−3 is less than 30 U mL^{-1} whereas high postsurgical serological levels (>30 U mL^{-1}) may indicate disease progression or recurrence.[7−9]

Traditional laboratory-based analytical assays for cancer biomarkers analysis rely on immunoassays,[10,11] such as enzyme-linked immunosorbent assay (ELISA), typically requiring labeling or additional reagents to monitor the binding event, making routine measurements inside hospitals rather laborious, time-consuming, expensive, having limited automation of procedures and normally requiring specialized personnel. Thus, the development of new sensing solutions is currently needed in the diagnosis field toward the label-free, fast, simple, cost-effective and automated screening of cancer biomarkers in laboratorial context, without compromising detection sensitivity, specificity, and reproducibility.

This work aims to develop a new fully automated biosensing methodology for detection of CA 15−3 in biological fluids, by merging the features of surface plasmon resonance (SPR) spectroscopy and electrochemical techniques (eSPR). Plasmonic biosensors are capable of monitoring interactions in real time between a recognition element immobilized on the surface of a metal film (such as gold) and a ligand (in solution).[12,13] Comparing to other biosensing methods, SPR technology offers the advantages of high robustness to external interferences, high degree of automation, stability in complex environments (including plasma, serum, and whole blood), possibility of parallel sensing and widespread surface chemistry procedures for effective attaching of bioreceptors (namely antibodies, proteins, oligonucleotide strands, MIPs, etc.), among others, which explains the large number of recent publications reporting new applications for SPR biosensors, including the early disease diagnosis.[14,15]

Although direct label-free SPR approach has been widely applied to study the properties and interactions of various biomolecules at solid surfaces,[12,13] the sensitivity of SPR

Received: December 22, 2020
Accepted: May 17, 2021
Published: May 26, 2021

https://doi.org/10.1021/acs.analchem.0c05367
Anal. Chem. 2021, 93, 7815−7824

Scheme 1. Schematic Representation of the eSPR Detection Approach Used in This Work for Detection of CA 15-3 Biomarker[a]

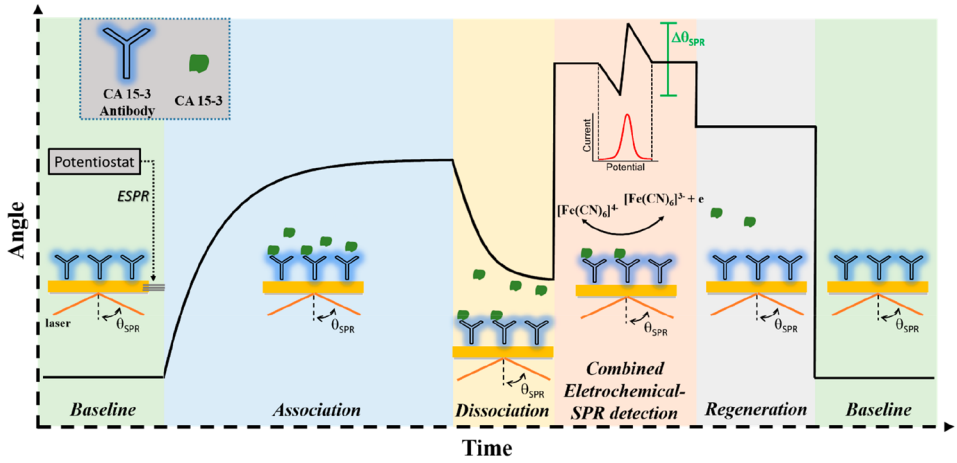

[a]For simplicity, antibody orientation was not taken into account in the detection scheme.

technique often needs to be improved when the amount of analyte bound to substrates induces insignificant refractive index variation and signal amplification strategies are commonly used to achieve biologically relevant concentration levels.[14,16] However, most of the amplification procedures is usually based on secondary antibodies (often conjugated with nanomaterials),[17,18] thus, requiring complex detection schemes and/or expensive chemical labels.[19,20] By opposition, the intrinsic high sensitivity, simplicity, and rapid response of electrochemical methods[21−23] can provide a suitable label-free and cost-effective amplification strategy to the SPR technique. From the experimental point of view, the thin metal film on substrates has the dual function of excite surface plasmons and act as working electrode for the electrochemical readout.

According to our bibliographic research, the combination of SPR with electrochemistry (eSPR) for analytical purposes is restricted to very few papers (refs 24, 25, 26, 27), which is probably related to the eSPR setup specificities and/or constrains related to the electrochemical response after surface modification with bioreceptors. Besides, the reported studies uses complex and expensive detection procedures since the measurable electrochemical signal arises from electroactive markers (i) generated in situ (coming from enzyme conjugated-secondary antibodies),[24] or (ii) covalently attached to secondary reporting biomolecules (such as proteins and oligonucleotides).[25,26] Recently, an innovative eSPR approach was developed by our research team for the ultrasensitive screening of miRNA-145.[4] Briefly, the detection procedure consisted in real-time SPR monitoring of the hybridization event followed by the potential-assisted deposition of a redox probe on the SPR sensor surface. Unlike the direct SPR monitoring of the binding assay, changes in optical properties induced by the electrochemical process afforded a much larger SPR response, thereby improving the detection sensitivity to femtomolar levels for application in clinical diagnosis context.

The innovative concept of this work is to combine optical and electrochemical responses in the same spot to detect and quantify CA 15−3 in biological samples, with high sensitivity (and selectivity), in a very simple, label-free, accurate, and fully automated manner. Detection was achieved by performing two simple steps (see Scheme 1). In the first detection step, direct SPR monitoring of interactions between CA 15−3 antigen in solution with surface immobilized antibody was performed until adsorption reached dynamic equilibrium. In the second detection step, incremental sensitivity to the binding assay was achieved by the electrochemical process. The more sensitive electrochemical response to the binding event was obtained by performing square wave voltammetry (SWV) measurements in the presence of a biocompatible redox probe.

EXPERIMENTAL SECTION

Materials and Solutions. Carbohydrate Antigen 15−3 (CA 15−3, 10.9 kU mL^{-1}) and purified anti-Mucin 1 rabbit polyclonal antibody (1 mg mL^{-1}) were purchased from EMELCA Bioscience and St Johńs Laboratory, respectively. Standard stock solutions of anti-CA 15−3 (50 μg mL^{-1}, in 10 mM PBS, pH 7.4) and CA 15−3 (1.0 kU mL^{-1}, in 10 mM acetate buffer solution, pH 4.0) were prepared and stored at −20 °C if not in use. Less concentrated solutions and standards were obtained from the previous solutions. Other chemicals, materials and solutions used throughout this work are described in the Supporting Information (SI).

Instrumentation. The complete eSPR setup used in this work, operation conditions and experimental details used for performing the electrochemical measurements in combination with SPR are described in the SI.

Immobilization of anti-CA 15−3 Antibody on SPR Sensor Surfaces. Self-assembled monolayers (SAMs) of mercaptosuccinic acid (MSA) on gold SPR substrates were prepared by immersing the clean sensor surfaces into a 1 mM MSA aqueous solution overnight. Afterward, the modified chips were rinsed with pure water and dried under a stream of N_2. Prior to the surface activation, successive injections of 10 mM acetate buffer solution (pH 4.5) and 100 mM HCl into the cuvette were performed (see SI Figure S1) to remove unbound thiol molecules and stabilize the MSA monolayer.

The preparation of the sensing surfaces (see SI Scheme S1) was performed by using SPR facilities to control the addition of all solutions into the cuvette in a full-automated manner, resulting in improved handling of reagents and samples, minimizing contaminations and operator errors. First, the baseline was collected with running buffer solution (10 mM PBS, pH 7.4), followed by MSA activation, by reaction of carboxylic groups with an equimolar mixture of *N*-(3-

https://doi.org/10.1021/acs.analchem.0c05367
Anal. Chem. 2021, 93, 7815−7824

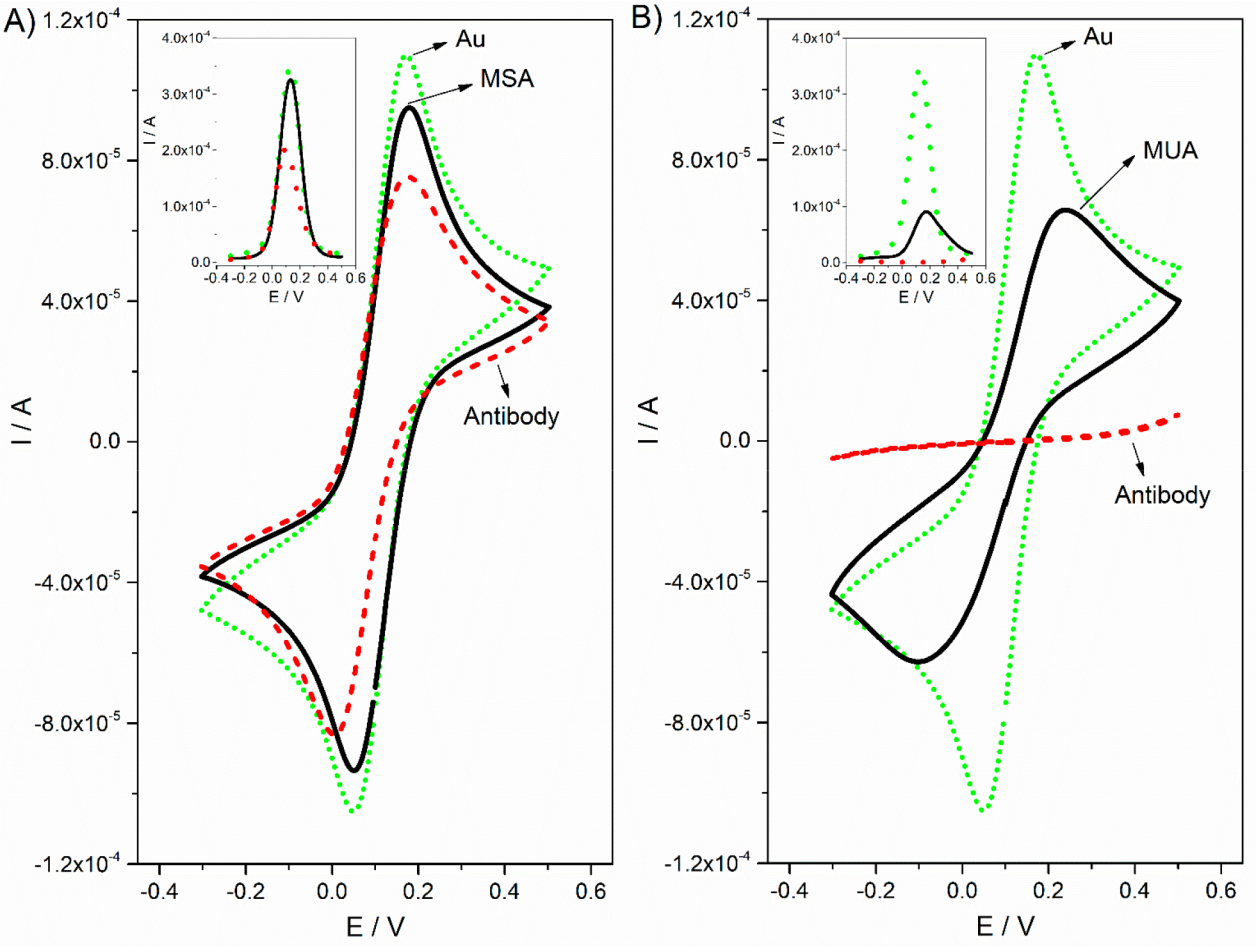

Figure 1. CVs obtained, in the presence of 5 mM $[Fe(CN)_6]^{3-/4-}$ redox pair, at the SPR gold surface previously modified with carboxylic-acid-terminated SAMs of (A) MSA and (B) MUA, (—) before and (---) after EDC/NHS coupling of CA 15−3 antibody. For comparison, the voltammograms collected at the bare Au surface were also included in the figure. Insets: SWVs obtained under the same experimental conditions.

dimethylaminopropyl)-*N*′-ethylcarbodiimide hydrochloride (EDC) and *N*-hydroxysuccinimide (NHS) in water (*C* = 50 mM), for 5 min. The mixture in then washed away with buffer solution. After activation of the MSA monolayer, antibody immobilization was achieved by incubation of the sensor surface for 15 min with a 20 μg mL^{-1} anti-Mucin 1 antibody solution, dissolved in 10 mM acetate buffer solution at pH 4.0 (coupling buffer). The sensor surface was then washed with running buffer solution to remove loosely bound material. After immobilization of CA 15−3 antibody, the gold surface was exposed to a 1 M ethanolamine solution (pH 8.0) for 10 min to deactivate unreacted reactive esters on the surface, following by surface wash with running buffer and SDS to reduce nonspecific binding (NSB).

CA 15−3 Detection by SPR and Electrochemical Responses. Before the interaction of CA 15−3 with covalently immobilized anti-CA 15−3 antibody on the SPR gold chips, the sensor surface was stabilized by repetitive injections of 10 mM PBS, pH 7.4 (see SI Figure S2).

Detection of CA 15−3 by combined optical and electrochemical measurements was carried out automatically by the Autolab ESPRIT robotic autosampler. After baseline collection in 10 mM PBS (pH 7.4) for 60 s, the sensor surface was incubated with standard solutions of CA 15−3, with concentrations ranging from 0.10 to 500 U mL^{-1}, and the binding event was monitored for 15 min by SPR (association). Then, the sensor surface was washed with background solution to remove unbound material (dissociation). In the following detection step, 50 μL of 5 mM ferro/ferricyanide solution was injected into to the cuvette to perform the electrochemical measurements. After 150 s equilibrium, a SWV measurement was recorded in the potential range of −0.3 to 0.5 V, followed by redox probe drain out from the measuring channel. Finally, a 0.1 M Gly-HCl (pH 2.0) solution was injected into the system for 5 min in order to regenerate the sensor surface between the analysis of CA 15−3 solutions with different concentration.

For comparative purposes, all sensorgrams obtained were normalized to a baseline value of zero and plotted in OriginLab (version 2016). The angle variation obtained under SPR binding equilibrium and the redox probe amperometric signals resulting from SWV measurements, for the various CA 15−3 concentrations tested, were used to build the calibration curves.

RESULTS AND DISCUSSION

In this work, SAM approach and SPR technique provided the construction of a generic sensor platform, which, in conjunction with appropriate biorecognition element, allowed performing eSPR experiments for detection of CA 15−3 in a reagentless, label-free and fully automated format (see Scheme 1). The CA 15−3 antibody immobilization on SPR gold

https://doi.org/10.1021/acs.analchem.0c05367
Anal. Chem. 2021, 93, 7815−7824

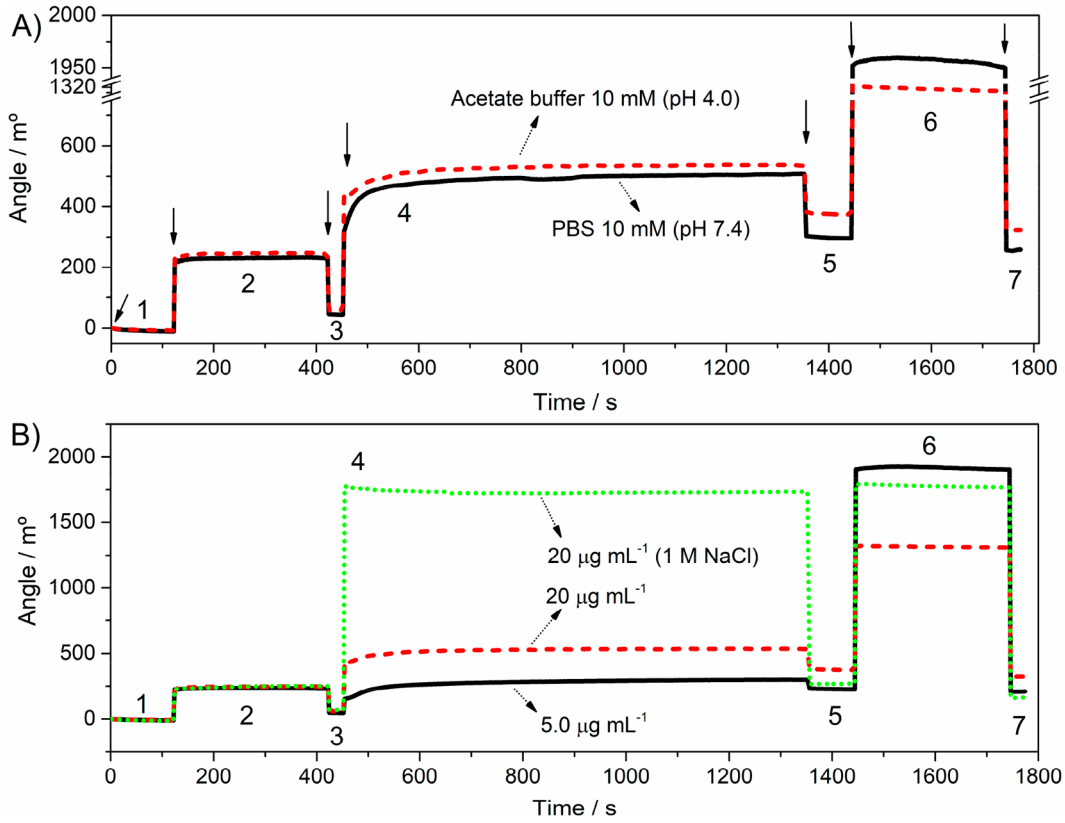

Figure 2. Effect of the (A) association buffer pH (for a 20 μg mL^{-1} CA 15−3 antibody solution), (B) concentration of the antibody and ionic strength of association medium (10 mM acetate buffer, pH 4.0) on the immobilization of CA 15−3 antibody on the SPR gold disk surface. Line 1: baseline collected in 10 mM PBS, pH 7.4, for 120 s; Line 2: activation of the carboxylic-acid-terminated SAM with a mixture of EDC/NHS (50 mM, in water); Line 3: wash with 10 mM PBS, pH 7.4, for 30 s (return to baseline); Line 4: immobilization of CA 15−3 antibody for 900 s; Line 5: wash with 10 mM PBS, pH 7.4, for 90 s (return to baseline); Line 6: deactivation of remaining reactive esters with 1 M ethanolamine (pH 8.0), for 300 s; Line 7: wash with 10 mM PBS, pH 7.4, for 30 s (return to baseline).

substrates and the eSPR measurements were performed by using a fully automated SPR injection sequence which results in fast, simple, and reproducible[28] preparation of sensor surfaces and detection procedures for screening of CA 15−3 cancer biomarker. Also, the optimization of surface bio-functionalization strategies was deeply considered on this work to enhance the performance of the eSPR bioassay based on combined SPR and electrochemical responses at the same sensor platform.

SAM Selection for the eSPR Measurements. In the first stage of construction, the type of alkanethiol that would form the self-assembled monolayer (SAM) was studied. In this work, three ω-carboxylic acid alkanethiols with different (i) chain length and/or (ii) number of carboxylic acid groups per molecule, MSA, 3-mercaptopropionic acid (3-MPA) and 11-mercaptoundecanoic acid (11-MUA), were tested as linker molecules for effective immobilization of the recognition element at the gold surface (see SI for details), while providing (i) maximal density of bioreceptors to increase the detection signal, (ii) effective reduction of NSB, and (iii) measurable and reversible redox probe electrochemical response.

The redox reaction taking place at the SAM electrode surface was evaluated first for the $[Fe(CN)_6]^{3-/4-}$ redox pair, using cyclic voltammetry (CV) and SWV techniques, as shown in Figure 1. As can be seen, a reversible diffusion-limited process was observed for the less organized MSA monolayer (before and after antibody immobilization; see Figure 1A) whereas no peak current was observed after antibody coupling to the well-ordered 11-MUA modified surface (see Figure 1B), compromising electrochemical measurements due to the formation of an electrically insulating monolayer that caused a greater barrier to redox probe penetration through the monolayer toward the electrode surface.

Antibody immobilization efficiency was also evaluated for both thiols by monitoring the optical response after the injection of a 20 μg mL^{-1} CA 15−3 antibody solution into the measuring system. The overall SPR angle variations obtained, after surface washing, were 414 ± 29 m° (see Figure 2) and 428 ± 35 m° (see SI Figure S3 and Figure S4A) for the short-chain and long-chain SAM, respectively, showing that antibody density at the SPR substrates was very similar for both systems tested. Although 11-MUA long-chain are more densely packed increasing bioreceptors immobilization,[29−31] the abundant functional −COOH groups (two per molecule) of the less dense MSA monolayer can probably contribute to a larger amount of antibodies immobilized. Relatively to 3-MPA, a lower SPR angle shift (of 199 ± 20 m°) was observed after antibody immobilization which can be explained by the fact that this less ordered (than 11-MUA) monolayer only contains one −COOH group per molecule. Furthermore, this lower antibody density seems to provide higher accessibility to antibodies recognition sites since the sensor response to 30 U mL^{-1} CA 15−3 was very similar for the three SAMs tested (see SI Figure S4B). However, although the MSA sensing platforms

https://doi.org/10.1021/acs.analchem.0c05367
Anal. Chem. 2021, 93, 7815−7824

can suffer from steric hindrance due to high antibody surface density, the larger number of − COOH groups (two per molecule) at the chip surface can provide, at least in theory, more ability to resist to NSB after blocking of unreacted NHS-ester groups with ethanolamine, which is essential for analysis of complex biological samples, such as serum. Thus, short thiol MSA showed to be suitable for integration into eSPR biosensors since it combines both, effective bioreceptor immobilization without excessive block to electron transfer for sensitive combined optical and electrochemical detection.

Antibody Immobilization on Sensor Surfaces. Immobilization of biorecognition elements on sensor surfaces plays an important role in sensor sensitivity and selectivity. Thus, efficient antibody immobilization procedures should be used (see SI Scheme S1), to provide stable baselines and improved sensor response during eSPR measurements.

For effective CA 15−3 antibody immobilization, the experimental conditions (association buffer composition, pH, antibody concentration, reaction times, etc.) were carefully optimized, as can be seen in Figure 2. CA 15−3 antibody solutions, diluted to concentration levels of 20 and 5 μg mL^{-1} in buffer solutions at pH 4.0 and pH 7.4 (see Figure 2A) and having different medium ionic strength (see Figure 2B), were injected individually over the sensor surface. Based on the resulting SPR signals, low ionic strength acidic buffer solution (10 mM Na-acetate buffer, at pH 4.0) was selected as association buffer. The results obtained suggests that some of the unreacted carboxylic acid groups, after EDC/NHS activation, remained negatively charged at the SAM surface (pK_a values of MSA and MUA lie in the range 3−5[32,33]) contributing to preconcentrate the positively charged amino acid residues in the anti-CA15−3 antibody. This electrostatic effect seems to be more notorious when the antibody is dissolved in acid buffer solution since a higher amount of antibody was bound. By opposition, the use of the high ionic strength buffer containing 1 M NaCl does not benefit from electrostatic attraction of antibodies to the sensing surface since hydrophobic mechanisms dominates,[34] thus, decreasing the amount of bioreceptors immobilized and further suggesting electrostatic attraction (in low ionic strength medium) as key mechanism for immobilization of proteins on the biosensing surfaces.[35−37] Furthermore, the optimal antibody concentration for the interaction study was found to be 20 μg mL^{-1}, based on the overall SPR angle variation after ligand coupling.

The overall immobilization process of the CA 15−3 antibody on the sensor surface, previously modified with an MSA SAM, is shown is Figure 3. Prior to antibody immobilization, the system baseline was collected in 10 mM PBS, pH 7.4. Then, the −COOH groups present at the monolayer surface were activated by incubation of the sensor surface with a mixture of EDC and NHS in water for 5 min, followed by surface wash with background solution. The measured SPR angle shifted to values around 100 m°, meaning that NHS-ester reactive groups were formed at the surface. After surface activation, a 20 μg mL^{-1} CA 15−3 antibody solution, dissolved in coupling buffer (10 mM acetate buffer, pH 4.0), was injected into the SPR cuvette for 15 min. The SPR angle rapidly increased with reaction time for the first few minutes, due to the rapid coupling of the antibody to the surface, after which the system tends to steady-state conditions. Loosely bound antibodies were then removed after passing background solution over the sensor surface for 90 s. After antibody immobilization, the remaining unreacted reactive

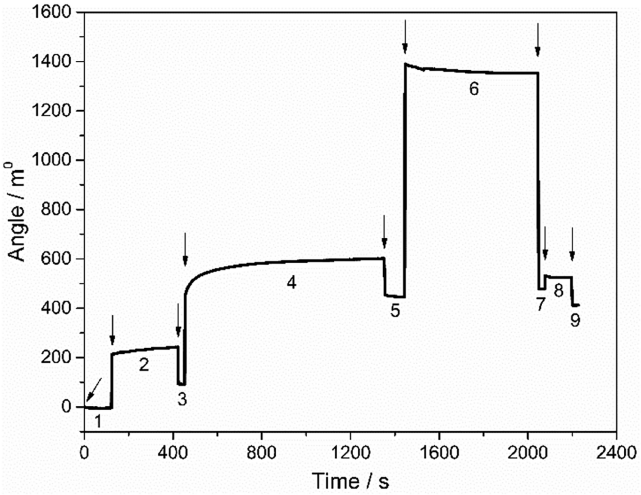

Figure 3. Representative sensorgram showing the different steps involved in the immobilization of CA 15−3 antibody on the MSA-modified SPR gold disk. Line 1: baseline collected in 10 mM PBS, pH 7.4, for 120 s; Line 2: activation of carboxylic-acid-terminated SAM with a mixture of EDC/NHS (50 mM, in water) for 300 s; Line 3: wash with 10 mM PBS, pH 7.4, for 30 s (return to baseline); Line 4: immobilization of CA 15−3 antibody (C = 20 μg mL^{-1}), dissolved in 10 mM acetate buffer solution, pH 4.0, for 900 s; Line 5: wash with 10 mM PBS, pH 7.4, for 90 s (return to baseline); Line 6: deactivation of remaining reactive esters with 1 M ethanolamine (pH 8.0) for 600 s; Line 7: wash with 10 mM PBS, pH 7.4, for 30 s (return to baseline); Line 8: wash with 10 mM PBS, pH 7.4, containing 0.1% SDS, for 120 s; Line 9: wash with 10 mM PBS, pH 7.4, for 30 s (return to baseline).

esters on the SAM surface were deactivated by reaction with 1 M ethanolamine (pH 8.0) for 10 min, followed by surface wash with buffer solution. As can be seen in the registered sensorgram, when initial conditions were restored, the measured SPR angle slightly increased when comparing with that obtained after antibody immobilization, revealing the successful surface block by ethanolamine. Finally, the sensor surface was treated with regeneration solution containing SDS (to remove antibodies that were nonspecifically bound to the chip surface) and then with background solution.

Automated procedures used for preparation of sensor surfaces by the SPR autosampler allowed to reduce batch-to-batch irreproducibility. Reproducibility of the immunoassay was evaluated by comparing the amount of immobilized antibody between 18 biosensor platforms, constructed under the same experimental conditions on different days. The relative standard deviation (RSD) value was 7.9%, indicating that the automated built process was reproducible.

Contact Angle, AFM and Ellipsometry Measurements. The SPR chip surface was also characterized by contact angle (CA), AFM, and ellipsometry analysis.

The wettability of the different layers composing the sensing surface was characterized by measuring the CA (see SI Figure S5A). The values obtained were 59.8 ± 0.7, 47.1 ± 0.8, and 51.8 ± 0.9 for bare, MSA-modified, and antibody-modified SPR chips, respectively. A large net decrease in CA was observed for the charged and hydrophilic MSA surface while a relatively small net increase was observed after CA 15−3 antibody immobilization, probably due to the extensive hydrophobic patches of the antibody. The overall increase in surface hydrophilicity was also reported by Çimen et al.[38] after immobilization of troponin I antibody on the SPR chips.

https://doi.org/10.1021/acs.analchem.0c05367
Anal. Chem. 2021, 93, 7815−7824

The buildup of the SPR sensing platforms was followed by AFM to examine the surface morphology and coverage of the deposited thin film. Yet, the 3D-images (see SI Figure S5B) showed an increase of the surface depth values (from 7.6 to 18 nm) which can be related to the increase in the film thickness, indicating that the antibody was homogeneously immobilized over the SAM surface.

Ellipsometry measurements were performed aiming to estimate the overall film thickness on the dried sensor surface. From the fits performed, a thickness value of 0.45 ± 0.01 nm was obtained for the MSA monolayer. After antibody immobilization on the preformed MSA SAM, the average thickness increased to 1.4 ± 0.4 nm (see SI Figure S5C). These results were of the same order of magnitude of thickness values reported for protein immobilization across different SAMs (from 0.45 to 2.3 nm)[35,39] and much inferior to biomolecules attachment to thicker polymeric surfaces (42.8 nm).[38] Furthermore, the ellipsometric thickness obtained was in close agreement with the thickness of the ultrathin film (3.6 nm) obtained by fitting the SPR reflectivity curves with WinSpall theoretical model (see SI Figure S5E).

Optimization of Experimental Conditions for Antibody−Antigen Interaction. Experimental conditions of the immunoassay, such as association buffer pH, incubation time, regeneration conditions, etc., were carefully optimized to achieve improved performance. To study the effect of the pH on the specific binding of CA 15−3 to the sensor surface, a pH variation study was performed between pH 3.0 and 8.0. Solutions of 500 U mL^{-1} CA 15−3 at different pH values were injected into the measuring system for 15 min. The SPR angle variation for each pH value tested is shown in Figure 4. As can be seen, the overall angle variation due to the binding event greatly increased, when more acidic conditions were used (pH 4.5 to 3.5). Taking into account that the isoelectric point of CA 15−3 protein is predicted to be between 3 and 5,[40] and considering the obtained data (Figure 4), we suspect that CA 15−3 becomes increasingly positively charged for medium pH < 5. This positive charge favors the electrostatic interactions with the epitope regions of its antibody, which are expected to be negatively charged, resulting in enhanced SPR response. For pH < 3.5, the angle variation decreases drastically probably because the acid residues at antibody binding sites became increasingly uncharged with decreasing pH, reducing the efficiency of the immunoreaction. Thus, we have chosen the pH 4.0 as the ideal pH for the (low ionic strength) association buffer.

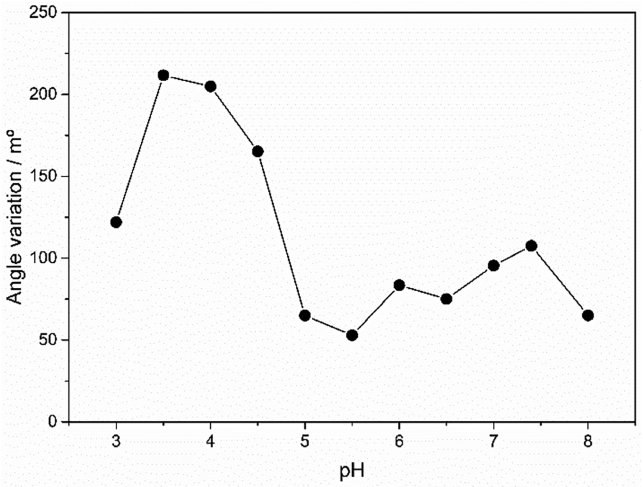

Figure 4. Effect of the pH of the association buffer solution on the SPR response after the interaction of 500 U mL^{-1} CA 15−3 with immobilized CA 15−3 antibody on the SPR gold disk for 15 min. Formic acid was used for pH 3.0 and buffer solutions used were: 10 mM acetate buffer for pH 3.5−5.5 and 10 mM PBS for pH 6.0−8.0.

In our detection studies, regeneration of the sensor surface was performed prior to the next binding event. After preliminary experiments, the best regeneration conditions were achieved by using a 0.1 M glycine-HCl buffer solution (pH 2.0), for 5 min (see SI Figure S6). No significant loss of antibody and/or reduction of its activity was observed for at least three consecutive runs.

Although the antibody coated surfaces were robust and allowed a repeated use after surface regeneration, thereby reducing cost per sample, some possible constrains related with the immunoassay performance were also identified. According to the literature, these include (i) the repetitive use of highly acidic regeneration solutions, which can denaturate immobilized biomolecules[41] and/or (ii) the instability of SAM surfaces promoted by usage over long periods of time (>24 h)[42] and/or (iii) the residues of redox probe on sensor surfaces that accumulate on continuous use and can permanently damage the electrode surface.[43,44] Thus, in this work, the most reliable and effective route for detection CA 15−3 biomarker was achieved by using freshly prepared eSPR sensing platforms to build calibration curves, taking advantage of (low-cost) disposable SPR gold chips.

Optical and Electrochemical Responses of the Immunosensor toward CA 15−3. The label-free and automated two-step immunoassay was carried out by incubation of the sensor surface with various standards of increasing CA 15−3 concentration (from 0.10 to 500 U mL^{-1}, in 10 mM acetate buffer solution, pH 4.0). In the first step, SPR technique was used for real-time monitoring of the selective interaction between CA 15−3 antigen and the surface immobilized anti-CA 15−3 antibody under the established optimal conditions, as can be seen in Figure 5A (left). First, the running buffer solution (10 mM PBS, pH 7.4) was injected into the SPR cuvette and the system baseline was collected for 60 s. Then, the sensor surface was incubated for 15 min with CA 15−3 standard solutions and adsorption reached dynamic equilibrium (steady-state conditions). The real-time SPR monitoring allowed the easy optimization of incubation time (before electrochemical measurements) for quicker analysis in clinical studies. After the formation of the stable complex, the surface was washed with background solution to remove unbound molecules.

The maximum SPR angle change resulting from the antigen−antibody interaction for the various CA 15−3 concentrations tested was used to build the calibration curve, shown in Figure 5B, after triplicate measurements (n = 3) for each antigen solution. As predicted from SPR equilibrium analysis theory,[24] a nonlinear dependence between the SPR intensity response with the amount of captured antigen was observed (see inset of Figure 5B). Thus, assay linearity was possible by plotting data as logarithmic concentration range (in U mL^{-1}),[24] in which two linear response ranges were obtained, ranging from 0.10 to 10 U mL^{-1} (R^2 = 0.981) and from 30 to 500 U mL^{-1} (R^2 = 0.987). However, the two sections presented different slopes since for low concentration levels, the angle shift is relatively slow while for higher concentrations

https://doi.org/10.1021/acs.analchem.0c05367
Anal. Chem. 2021, 93, 7815−7824

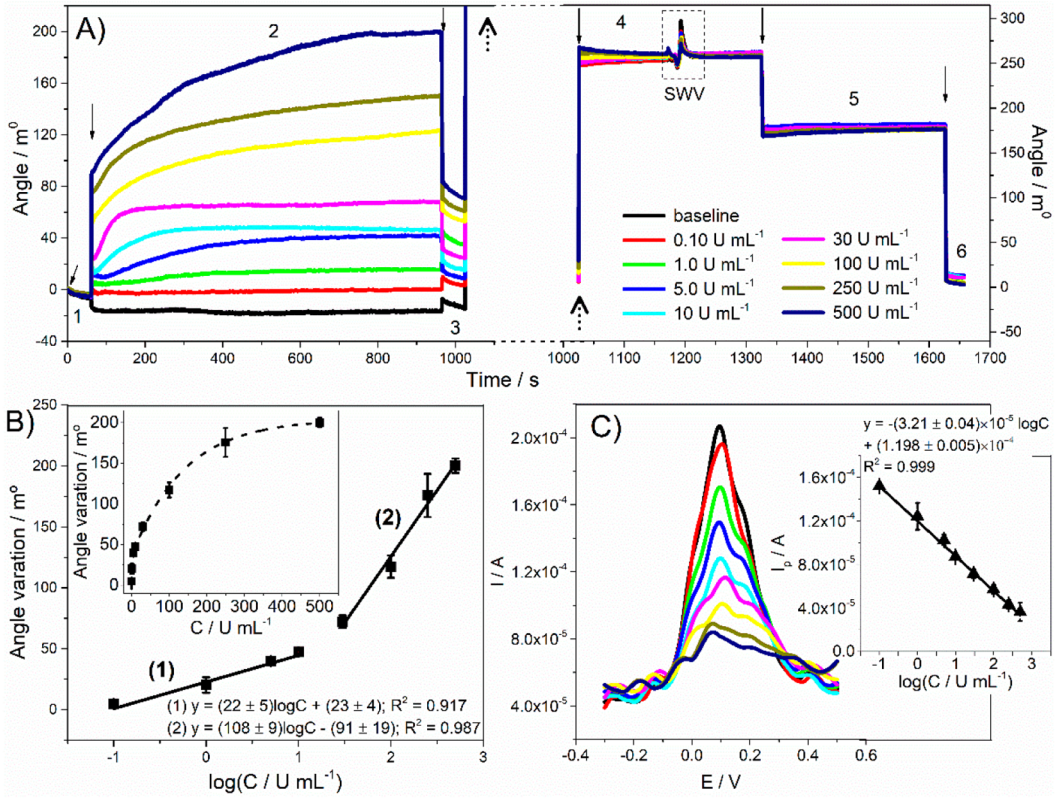

Figure 5. (A) Real-time SPR monitoring of the interaction between immobilized antibody on SPR gold substrates and CA 15−3 in solution (left) followed by electrochemical control (SWV)-SPR measurement in the presence of a redox probe (right). The concentrations of CA 15−3 tested ranged from 0.10 to 500 U mL^{-1}. Line 1: baseline collected in 10 mM PBS, pH 7.4, for 60 s; Line 2: real-time monitoring of the antigen−antibody interaction for 15 min; Line 3: surface wash with 10 mM PBS, pH 7.4, for 60 s (return to baseline); For comparison, the response obtained after injection of association buffer (10 mM acetate buffer solution, pH 4.0, without CA 15−3) into the measuring channel (dashed line) is also shown in the figure; Line 4: combined electrochemical control and SPR detection after injection of 5 mM ferro/ferricyanide redox probe into the measuring channel. After 150 s equilibration, a SWV measurement between −0.3−0.5 V (vs. Ag/AgCl) was performed; Line 5: surface regeneration after wash with glycine-HCl buffer solution (pH 2.0) for 300 s; Line 6: wash with 10 mM PBS, pH 7.4, for 60 s (return to baseline). (B) Graphical representation of the obtained SPR angle variation as a function of the CA 15−3 concentration (inset) and logarithm of the CA 15−3 concentration. (C) SWV voltammograms collected in step 4. Inset: graphical representation of the redox probe peak current (I_p) as a function of the logarithm of the CA 15−3 concentration. Error bars correspond to standard deviations of analytical signals collected from three independent immunoassays.

(midrange region of the typical S-shaped curve) the angle variation increases significantly. The interception of these two linear segments allowed the LOD estimation. From the plot, the detection limit (LOD) was estimated to be 21 U mL^{-1}. This value of LOD was obtained according to Recommendations of IUPAC for ion-selective electrodes,[45] in which calibration plots also use log(concentration).

In the second detection step, electrochemical measurements in the presence of a biocompatible redox probe were performed after direct monitoring of the binding event. SWV technique was selected for the amperometric readout since this technique has been widely used for the detection of disease biomarkers with high sensitivity and fast measuring time (few seconds only).[21,46] To do so, a 5 mM ferro/ferricyanide solution was first injected into the measuring channel. After 150 s equilibrium, along which no potential was applied to the cell, the current generated by the oxidation of the redox couple was recorded from −0.3 to 0.5 V (vs. Ag/AgCl). The voltammograms were collected under hydrodynamic conditions since the Autolab ESPRIT integrated syringe provides continuous aspirating/dispensing cycles of the redox probe solution into the cuvette, which greatly increases the mass transport at the surface. Moreover, it is also important to notice that SPR angle chances induced by the electrochemical process was also considered for analytical purposes (see SI Figure S7), however, the high variability of the SWV-induced SPR angle variation resulted in very low assay linearity. Finally, the redox probe was washed-out from the cell and regeneration of the sensing surface was achieved by incubation in a 0.1 M Gly-HCl solution (pH 2.0), for 5 min, followed by surface wash with PBS.

The SWV voltammograms collected are displayed in Figure 5C and show a peak current decrease with the increasing CA 15−3 concentration due to electron transfer inhibition after the formation of antibody−antigen imunnocomplexes at the electrode surface. In addition, the resulting redox probe peak currents were plotted as function of the increment of CA 15−3 logarithm concentration (see inset of Figure 5C). Good linearity of calibration curve (R^2 = 0.999) was achieved from 0.10 to 500 U mL^{-1}, with an LOD[45] of 0.0998 U mL^{-1}. Thus, the sensitivity (and accuracy) of the electrochemical approach for screening CA 15−3 antigen is much superior to the obtained by direct SPR sensing (about ∼210 times), emphasizing the important contribution of electrochemical detection to plasmonic biosensors toward the quantification of low levels of cancer biomarker. These results were consistent

https://doi.org/10.1021/acs.analchem.0c05367
Anal. Chem. 2021, 93, 7815−7824

with other eSPR immunosensors reported in literature, where lower detection levels were achieved by electrochemical readout relatively to SPR detection.[24,47] Furthermore, the LOD obtained by the developed eSPR biosensor is (i) lower than that obtained by commercially available ELISA kits and (ii) of the same order of magnitude of LODs recently reported in literature by other immunoassays for detection of CA 15−3 biomarker (see SI Table S1). In addition, the developed eSPR methodology has also one of the widest concentration range of response reported, allowing direct analysis of samples well above the cutoff value (of 30 U mL^{-1}),[7−9] which may be very important when following the progress of treatment.

Also comparing with the literature, the amplification strategies of the reported immunosensors for screening CA 15−3 (see SI Table S1) are usually based on either secondary antibodies and/or metal/magnetic NPs or nanocomposites. These approaches may have some limitations, such as laborious and time-consuming procedures, need of expensive chemical labels, problematic removal of unbound label, steric hindrance, instability, limited application in complex biological samples, among others.

Focusing on the demonstration of the eSPR approach for label-free biosensing, the results obtained were compared with other label-free sensing techniques reported in the literature. In this context, a new SPR optical platform based on $Au_{(50\ nm)}$/$ZnO_{(50\ nm)}$ films, fabricated by radio frequency sputtering technology, showed high detection sensitivity (LOD = 0.025 U mL^{-1}, 4 times lower than $Au_{(50\ nm)}/Cr_{(2\ nm)}$ layers).[48] However, despite the great potential of ZnO nanostructures for signal enhancement, these SPR chips are not commercially available. Recently, the catalytic activity of a CuS/reduced graphene oxide nanocomposite was employed for label-free electrochemical detection of CA 15−3 and the LOD obtained (of 0.3 U mL^{-1})[49] was similar to the obtained in this work. Thus, in our opinion, our simple and label-free eSPR methodology can provide an extremely attractive way of sensing CA 15−3, especially considering sensitivity, simplicity, time of analysis, and operational point of views.

Control experiments were performed to study the nonspecific attachment of species to the sensor surface under the experimental conditions tested. In these experiments, association buffer (without CA 15−3) and redox probe solution were successively injected over the sensor surface and the optical and electrochemical responses recorded (see SI Figures S8 and S9). No significant response variation was observed, revealing poor contribution of NSB of buffer and redox probe solutions to the detected signals.

Selectivity of the eSPR Biosensor. The quality of the developed eSPR immunosensor depends on the affinity and selectivity of the antibody to its antigen. In this work, the selectivity of the bioassay was evaluated by recording the SPR response for detecting CA 15−3 (C = 30 U mL^{-1}) in the absence and presence of other common cancer biomarkers, namely CA 125 (C = 15 U mL^{-1}), CA 19−9 (C = 25 U mL^{-1}), and CEA (C = 10 ng mL^{-1}) (see SI Figure S10). Compared with pure CA 15−3 buffer solution, the angle change recorded for the mixed solution was very similar (change in response was only 7.3%). Thus, the interfering biomarkers tested did not evidently interact with the immobilized polyclonal antibody and/or with CA 15−3 in solution (cross-reactivity), showing that the eSPR immunosensor is highly selective to the CA 15−3 tumor marker.

Application to Serum Samples Analysis. To obtain clinically relevant results, the developed eSPR detection methodology was applied to the detection of CA 15−3 in human serum samples. SPR detection of biomarkers in serum samples is particularly challenging, due to its complexity and problems arising from NSB of serum proteins can compromise label-free detection[50−54] due to the largely uncontrolled background signals (typically much higher when compared to the pure buffer solution). In this work, preliminary experiments were performed to carefully adjust the experimental conditions (see details in SI) to the analysis of serum.

Serum samples were prepared by simple dilution in a NSB hindering buffer composed of 10 mM phosphate buffer solution (PBS), at pH 7.4, supplemented with 0.1% Tween 20 (PBST), 0.5 M NaCl and 200 μg mL^{-1} of BSA (PBST-BSA). Serum samples were diluted 100 times. Furthermore, the following protocol was adopted to perform the detection assay in human serum: (i) first, the gold chip was stabilized with successive injections of PBST-BSA buffer for continuous blocking of the unoccupied areas of the gold surface; (ii) then, two diluted serum sample solutions (without CA 15−3) were successively injected over the sensor surface in order to further minimize NSB of serum proteins (see SI Figure S11A); (iii) finally, nonpathological serum samples spiked with different known concentrations of CA 15−3 were analyzed to build the calibration curve.

After the blocking procedure was carried out, the optical and electrochemical responses to the binding event in human serum samples were very different. SPR detection had limited success as biosensing technique probably due to (i) lower amount of CA 15−3 bound under the assay conditions (physiological pH and high ionic strength) and less favorable electrostatic interactions with the chip surface since serum does not significantly affect the ionization state of CA 15−3 (comparing to acidic buffer solution) and; (ii) some possible matrix interference. However, the high sensitivity of electrochemical detection was able to provide good results regarding the reliable detection of CA 15−3 in serum samples. Based on the calibration plot obtained (see SI Figure S11B), the analytical performance of the eSPR immunosensor in human serum was estimated. The linear range is from 0.10 to 250 U mL^{-1} and an LOD of 0.098 U mL^{-1} was obtained. Because of sample dilution in NSB hindering buffer, the LOD obtained corresponds to an original undiluted serum sample CA 15−3 concentration of 9.8 U mL^{-1}. Thus, the enhanced sensitivity of electrochemical techniques allowed the analysis of CA 15−3 in human serum at clinically relevant levels (CA 15−3 cutoff value: 30 U mL^{-1}[7−9]), while having an acceptable linear concentration range to provide clinically relevant information about progression and recurrence of breast carcinoma.

Moreover, the use of electrochemical readout as signal amplification strategy was able to overcome some major technical difficulties associated to SPR studies in complex biological samples, such as the refractive index mismatch from the different solutions (running buffer/dilution buffer/samples) injected into the measuring system and/or the need of a control serum solution injected into the reference channel to perform the assay. To evaluate the applicability of the proposed eSPR biosensor, recovery studies were performed (see SI Table S2I). Average detection recoveries between 91.2% and 105.4% (with an average relative error of 5.9%) were obtained, revealing a good relationship between added and found amounts of CA15−3. Overall, our electrochemical-

https://doi.org/10.1021/acs.analchem.0c05367
Anal. Chem. 2021, 93, 7815−7824

combined SPR detection methodology was a promising tool for the sensitive and label-free detection of CA15−3 in real biological samples.

CONCLUSIONS

This work describes a novel label-free, simple, and sensitive detection methodology for screening the breast cancer biomarker CA 15−3, based on the response from two detection systems, SPR and electrochemical techniques, in the same immunosensing spot. The eSPR immunoassay required minimal reagent/sample amounts and the SPR robotic autosampler allowed fully automated in situ preparation of the sensing platforms and detection procedures, a unique advantage for analysis in clinical laboratories. The total assay time (real-time SPR measurement, electrochemical measurement, and sensor regeneration) was around 30 min per sample. In addition, the incubation time can be optimized during the real-time SPR monitoring to reduce the assay period.

Results obtained after optimization of the eSPR bioassay in spiked buffer solutions revealed that electrochemical techniques can provide a suitable amplification strategy to direct SPR sensing, lowering the detection levels achieved without the need of additional complex and/or expensive amplification steps to enhance the sensitivity. The high sensitivity achieved by the electrochemical approach allowed the detection of concentration levels of CA 15−3 of about ∼210 times lower than that of the optical readout. Also, the selectivity studies performed revealed that the immunoassay was able to discriminate CA 15−3 in the presence of other common cancer biomarkers.

The applicability of the eSPR detection methodology in clinical diagnosis context was evaluated by the analysis of CA 15−3 in human serum. These studies allowed validating the use of electrochemical technique as label-free amplification strategy since NSB of serum proteins caused serious limitations to the SPR readings (lack of sensitivity). Thus, the antifouling surface chemistry strategies employed in this work were fundamental to minimize matrix effects. Samples were diluted in a NSB hindering buffer and no other pretreatment was employed. After surface blocking, the enhanced sensitivity of electrochemical readout allowed the reliable detection of CA 15−3 at relevant concentration levels to provide valuable information in clinical diagnosis context.

Overall, the use of real-time SPR detection technology integrating the high-performance electrochemical readout can bring important improvements to health diagnosis, as potential useful diagnostic tool in clinical laboratories and being an alternative to routinely used immunoassays for detection and monitoring of disease biomarkers.

ASSOCIATED CONTENT

Supporting Information

The Supporting Information is available free of charge at https://pubs.acs.org/doi/10.1021/acs.analchem.0c05367.

Chemicals, solutions, instrumentation, stabilization process o the Au/MSA surface, schematic representation of the CA 5−3 antibody immobilization on the SPR gold platforms, SPR bioplatforms stabilization process, SPR experiments at the MUA/Au surface, surface regeneration of the sensor suface, SPR response to the combined electrochemical control-SPR monitoring, immunosensors reported in the literature for the detection of CA 15−3, SPR and electrochemical responses in buffer solution (without CA 15−3), selectivity study, SPR response for successive injections of serum samples (without CA 15−3), calibration curve obtained in diluted human serum samples (PDF)

AUTHOR INFORMATION

Corresponding Authors

José A. Ribeiro − *CIQUP − Chemistry Research Center, Department of Chemistry and Biochemistry, Faculty of Sciences of University of Porto, 4169-007 Porto, Portugal;* orcid.org/0000-0001-6421-9763; Email: jose.ribeiro@fc.up.pt

Carlos M. Pereira − *CIQUP − Chemistry Research Center, Department of Chemistry and Biochemistry, Faculty of Sciences of University of Porto, 4169-007 Porto, Portugal;* orcid.org/0000-0002-8392-9581; Email: cmpereir@fc.up.pt

Author

Maria Goreti F. Sales − *BioMark@UC, Department of Chemical Engineering, Faculty of Sciences and Technology, Coimbra University, 3030-790 Coimbra, Portugal; Centre of Biological Engineering, Minho University, 4710-057 Braga, Portugal;* orcid.org/0000-0001-9936-7336

Complete contact information is available at: https://pubs.acs.org/10.1021/acs.analchem.0c05367

Notes

The authors declare no competing financial interest.

ACKNOWLEDGMENTS

This research had the financial support of FCT (Fundação para a Ciência e Tecnologia) and cofinanced by the European Union (FEDER funds) under the Partnership Agreement PT2020, Research Grants Pest-C/QUI/UIDB/00081/2020 (CIQUP) and NORTE-01-0247-FEDER-017834 (project RamSERS). J.A.R. (ref SFRH/BPD/105395/2014) and C.M.P. (ref SFRH/BSAB/150320/2019) acknowledge FCT under the QREN − POPH − Advanced Training, subsidized by European Union and national MEC funds. We thank BioMark/ISEP researchers Felismina Moreira and Joana Guerreiro for all the support to perform the ellipsometry measurements.

REFERENCES

(1) Ferlay, J.; Colombet, M.; Soerjomataram, I.; Mathers, C.; Parkin, D. M.; Pineros, M.; Znaor, A.; Bray, F. *Int. J. Cancer* **2019**, *144* (8), 1941−1953.

(2) Hayes, D. F. *N. Engl. J. Med.* **2019**, *381* (13), 1284−1286.

(3) Li, S. C.; Yang, X. R.; Yang, J. M.; Zhen, J. S.; Zhang, D. C. *Clinical and Experimental Medicine* **2016**, *16* (1), 29−35.

(4) Ribeiro, J. A.; Sales, M. G. F.; Pereira, C. M. *Sens. Actuators, B* **2020**, *316*, 128129.

(5) Lin, Z. Q.; Neiswender, J.; Fang, B.; Ma, X. L.; Zhang, J.; Hu, X. Y. *Oncotarget* **2017**, *8* (16), 26625−26636.

(6) Sturgeon, C. M.; Duffy, M. J.; Stenman, U.-H.; Lilja, H.; Brünner, N.; Chan, D. W.; Babaian, R.; Bast, R. C.; Dowell, B.; Esteva, F. J.; Haglund, C.; Harbeck, N.; Hayes, D. F.; Holten-Andersen, M.; Klee, G. G.; Lamerz, R.; Looijenga, L. H.; Molina, R.; Nielsen, H. J.; Rittenhouse, H.; Semjonow, A.; Shih, I.-M.; Sibley, P.; Sölétormos, G.; Stephan, C.; Sokoll, L.; Hoffman, B. R.; Diamandis, E. P. *Clin. Chem.* **2008**, *54* (12), No. e11.

(7) Duffy, M. J.; Duggan, C.; Keane, R.; Hill, A. D. K.; McDermott, E.; Crown, J.; O'Higgins, N. *Clin. Chem.* **2004**, *50* (3), 559.
(8) Chourin, S.; Georgescu, D.; Gray, C.; Guillemet, C.; Loeb, A.; Veyret, C.; Basuyau, J. P. *Annals of Oncology* **2009**, *20* (5), 962−964.
(9) Sölétormos, G.; Nielsen, D.; Schiøler, V.; Mouridsen, H.; Dombernowsky, P. *Eur. J. Cancer* **2004**, *40* (4), 481−486.
(10) Mordente, A.; Meucci, E.; Martorana, G. E.; Silvestrini, A., Cancer Biomarkers Discovery and Validation: State of the Art, Problems and Future Perspectives. In *Advances in Cancer Biomarkers: From Biochemistry to Clinic for a Critical Revision*; Scatena, R., Ed.; Springer Netherlands: Dordrecht, 2015; pp 9−26.
(11) Vaisocherová, H.; Homola, J., SPR Biosensors for Medical Diagnostics. In *Surface Plasmon Resonance Based Sensors*, Homola, J., Ed.; Springer Berlin Heidelberg: Berlin, Heidelberg, 2006; pp 229−247.
(12) Patching, S. G. *Biochim. Biophys. Acta, Biomembr.* **2014**, *1838* (1), 43−55.
(13) Homola, J. *Chem. Rev.* **2008**, *108* (2), 462−493.
(14) Masson, J.-F. *ACS Sensors* **2017**, *2* (1), 16−30.
(15) Bellassai, N.; D'Agata, R.; Jungbluth, V.; Spoto, G. *Front. Chem.* **2019**, *7*, 570.
(16) Chen, Y. X.; Huang, K. J.; Niu, K. X. *Biosens. Bioelectron.* **2018**, *99*, 612−624.
(17) Ekgasit, S.; Thammacharoen, C.; Yu, F.; Knoll, W. *Anal. Chem.* **2004**, *76* (8), 2210−2219.
(18) Homola, J.; Yee, S. S.; Gauglitz, G. *Sens. Actuators, B* **1999**, *54* (1), 3−15.
(19) Heaton, R. J.; Peterson, A. W.; Georgiadis, R. M. *Proc. Natl. Acad. Sci. U. S. A.* **2001**, *98* (7), 3701−3704.
(20) Wood, S. J. *Microchem. J.* **1993**, *47* (3), 330−337.
(21) Ricci, F.; Adornetto, G.; Palleschi, G. *Electrochim. Acta* **2012**, *84*, 74−83.
(22) Felix, F. S.; Angnes, L. *Biosens. Bioelectron.* **2018**, *102*, 470−478.
(23) Topkaya, S. N.; Azimzadeh, M.; Ozsoz, M. *Electroanalysis* **2016**, *28* (7), 1402−1419.
(24) Dong, H.; Cao, X. D.; Li, C. M.; Hu, W. H. *Biosens. Bioelectron.* **2008**, *23* (7), 1055−1062.
(25) Liu, J.; Tian, S.; Tiefenauer, L.; Nielsen, P. E.; Knoll, W. *Anal. Chem.* **2005**, *77* (9), 2756−2761.
(26) Dallaire, A. M.; Patskovsky, S.; Vallee-Belisle, A.; Meunier, M. *Biosens. Bioelectron.* **2015**, *71*, 75−81.
(27) Sriwichai, S.; Janmanee, R.; Phanichphant, S.; Shinbo, K.; Kato, K.; Kaneko, F.; Yamamoto, T.; Baba, A., Development of an electrochemical-surface plasmon dual biosensor based on carboxylated conducting polymer thin films. *J. Appl. Polym. Sci.* **2018**, *135* (1).45641
(28) Kausaite, A.; van Dijk, M.; Castrop, J.; Ramanaviciene, A.; Baltrus, J. P.; Acaite, J.; Ramanavicius, A. *Biochem. Mol. Biol. Educ.* **2007**, *35* (1), 57−63.
(29) Ayela, C.; Roquet, F.; Valera, L.; Granier, C.; Nicu, L.; Pugniere, M. *Biosens. Bioelectron.* **2007**, *22* (12), 3113−3119.
(30) Briand, E.; Salmain, M.; Compere, C.; Pradier, C. M. *Colloids Surf., B* **2006**, *53* (2), 215−224.
(31) Subramanian, A.; Irudayaraj, J.; Ryan, T. *Biosens. Bioelectron.* **2006**, *21* (7), 998−1006.
(32) Berchmans, S.; Nirmal, R. G.; Prabaharan, G.; Mishra, A. K.; Yegnaraman, V. *J. Solid State Electrochem.* **2006**, *10* (7), 439−446.
(33) Krolikowska, A.; Bukowska, J. *J. Raman Spectrosc.* **2007**, *38* (7), 936−942.
(34) Buijs, J.; White, D. D.; Norde, W. *Colloids Surf., B* **1997**, *8* (4), 239−249.
(35) Pei, Z.; Anderson, H.; Myrskog, A.; Dunér, G.; Ingemarsson, B.; Aastrup, T. *Anal. Biochem.* **2010**, *398* (2), 161−168.
(36) Löfås, S.; McWhirter, A., The Art of Immobilization for SPR Sensors. In *Surface Plasmon Resonance Based Sensors*; Homola, J., Ed.; Springer Berlin Heidelberg: Berlin, Heidelberg, 2006; pp 117−151.
(37) Löfås, S.; Johnsson, B.; Edström, Å.; Hansson, A.; Lindquist, G.; Hillgren, R.-M. M.; Stigh, L. *Biosens. Bioelectron.* **1995**, *10* (9), 813−822.
(38) ćimen, D.; Bereli, N.; Günaydın, S.; Denizli, A. *Talanta* **2020**, *219*, 121259.
(39) Phan, H. T. M.; Bartelt-Hunt, S.; Rodenhausen, K. B.; Schubert, M.; Bartz, J. C. *PLoS One* **2015**, *10* (10), No. e0141282.
(40) Wu, J.; Yan, Y.; Yan, F.; Ju, H. *Anal. Chem.* **2008**, *80* (15), 6072−6077.
(41) Mistry, K. K.; Layek, K.; Mahapatra, A.; RoyChaudhuri, C.; Saha, H. *Analyst* **2014**, *139* (10), 2289−2311.
(42) Srisombat, L.; Jamison, A. C.; Lee, T. R. *Colloids Surf., A* **2011**, *390* (1), 1−19.
(43) Vogt, S.; Su, Q.; Gutierrez-Sanchez, C.; Noll, G. *Anal. Chem.* **2016**, *88* (8), 4383−4390.
(44) Ribeiro, J. A.; Silva, E.; Moreira, P. S.; Pereira, C. M. *Chemistry Select* **2020**, *5* (17), 5041−5048.
(45) Buck, R. P.; Lindner, E. *Pure Appl. Chem.* **1994**, *66*, 2527.
(46) Wujcik, E. K.; Wei, H.; Zhang, X.; Guo, J.; Yan, X.; Sutrave, N.; Wei, S.; Guo, Z. *RSC Adv.* **2014**, *4* (82), 43725−43745.
(47) Kurita, R.; Nakamoto, K.; Ueda, A.; Niwa, O. *Electroanalysis* **2008**, *20* (20), 2241−2246.
(48) Chang, C.-C.; Chiu, N.-F.; Lin, D. S.; Chu-Su, Y.; Liang, Y.-H.; Lin, C.-W. *Anal. Chem.* **2010**, *82* (4), 1207−1212.
(49) Amani, J.; Khoshroo, A.; Rahimi-Nasrabadi, M. *Microchim. Acta* **2018**, *185*, 79.
(50) Eletxigerra, U.; Martinez-Perdiguero, J.; Barderas, R.; Pingarrón, J. M.; Campuzano, S.; Merino, S. *Anal. Chim. Acta* **2016**, *905*, 156−162.
(51) Martinez-Perdiguero, J.; Retolaza, A.; Bujanda, L.; Merino, S. *Talanta* **2014**, *119*, 492−497.
(52) Uludag, Y.; Tothill, I. E. *Anal. Chem.* **2012**, *84* (14), 5898−5904.
(53) Treviño, J.; Calle, A.; Rodríguez-Frade, J. M.; Mellado, M.; Lechuga, L. M. *Talanta* **2009**, *78* (3), 1011−1016.
(54) Situ, C.; Wylie, A. R. G.; Douglas, A.; Elliott, C. T. *Talanta* **2008**, *76* (4), 832−836.

https://doi.org/10.1021/acs.analchem.0c05367
Anal. Chem. 2021, 93, 7815−7824